Available online at www.sciencedirect.com
SCIENCE DIRECT®
PERGAMON
International Journal of Heat and Mass Transfer 46 (2003) 2219–2238
International Journal of HEAT and MASS TRANSFER
www.elsevier.com/locate/ijhmt

Surfactant effects on passive scalar transport in a fully developed turbulent flow

R.A. Handler [a,*], R.I. Leighton [a], G.B. Smith [a], Ryuichi Nagaosa [b]

[a] *Naval Research Laboratory, Washington, DC 20375, USA*
[b] *National Institute of Advanced Industrial Science and Technology, Tsukuba 305-8569, Japan*

Received 4 March 2002; received in revised form 20 September 2002

Abstract

Direct numerical simulations of fully developed turbulence in an open channel were performed. Effects of surfactants on heat transfer and the underlying turbulent structures were investigated. As surface elasticity is increased turbulent fluctuations are damped and the mean surface temperature is decreased. A surface strain model is introduced to explain this behavior in a heuristic manner. A nondimensional parameter representing the ratio of surface elastic forces to local inertial forces is introduced. It is concluded that for values of the parameter of order one, surfactants have strong effects on surface turbulence, whereas an effectively clean surface can be obtained for parameter values less than $O(10^{-3})$. Published by Elsevier Science Ltd.

Keywords: Surfactant; Turbulence; Direct numerical simulation; Infrared imagery

1. Introduction

It is well known that surfactants can have significant effects on the dynamics of free surfaces. Their ability to strongly damp capillary waves [1] is perhaps the most well known of these effects, and the mechanisms involved in this process have been the subject of many investigations. In this regard, recent work [2] has shown a clear relationship between the existence of natural surface films on the ocean surface and reduced radar backscatter from satellite based systems. It has also been known for some time, since the early work of Rideal [3], that surfactants can reduce evaporative heat transport at free surfaces. In addition to the above mentioned effects, recent simulations by Tsai [4] have shown that surfactants can significantly reduce the level of subsurface turbulence. Recent experiments by Saylor et al. [5,6] in which a surfactant was applied to a buoyancy driven turbulent flow cooled from above, clearly demonstrated that surfactants have a strong effect on the structure of the near surface turbulence. These effects included the damping of smaller scale turbulent structures, and a reduction in the average surface temperature. In these experiments, a so-called liquid phase surfactant was used [7] which caused no reduction in evaporative cooling. The experiments [5,6] point to the ability of surfactants to change the nature of near surface flows in addition to their known capacity to dampen surface waves or lessen evaporative cooling. We wish to explore these turbulence damping properties in the current work.

Additional motivation for our present work stems from the need to accurately determine sea surface temperatures and heat fluxes through infrared sensing of the ocean surface [8–10]. In these applications, the proper interpretation of surface temperature imagery is also an important goal. In this regard, naturally occurring surfactants may be expected to change the surface temperature. It may be anticipated, for example, that reducing latent heat transport would cause the surface temperature to rise in comparison to the surface temperature in uncontaminated regions. However, the situation is complicated by the fact that surfactants also reduce the intensity of subsurface turbulence, thereby increasing the thermal boundary layer thickness. This thickening alone, assuming constant heat flux from the

* Corresponding author. Tel.: +1-202-767-2457; fax: +1-202-767-3303.
E-mail address: handler@nrl.navy.mil (R.A. Handler).

0017-9310/03/$ - see front matter Published by Elsevier Science Ltd.
doi:10.1016/S0017-9310(02)00526-4

Nomenclature

A	slope of surface tension-concentration curve
b_{sf}, b_{surf}	expansion coefficients for vertical velocity
c_{ns}, c_{surf}	expansion coefficients for vertical velocity
d_{ns}, d_{sf}	expansion coefficients for vertical velocity
D	channel height
E	surfactant elasticity
f	driving pressure gradient
k	thermal conductivity
K	kinetic energy of an eddy per unit width
l^+	viscous or inner length scale
L_x, L_y, L_z	length scales of computational domain
L_E	length scale of typical turbulent eddy
Ma	Marangoni number
Nu	Nusselt number
p	pressure
Pr	Prandtl number
Pe	Peclet number
q_0	heat flux applied at free surface
R^*	Reynolds number
S	surface divergence
t	time
t^*	nondimensional time scale
$\bar{t}$	nondimensional time
T_c	convective time scale
T_d	dissipation time scale
u, v, w	components of velocity
u^+, v^+, w^+	nondimensional components of velocity
u', v', w'	components of the fluctuating velocity
u^*	velocity scale
u_{rms}, v_{rms}, w_{rms}	root mean square velocities
u_s	streamwise component of velocity at the free surface
U^+	nondimensional mean streamwise velocity
U_E	characteristic velocity of an eddy
$\mathbf{v}$	velocity field
$\mathbf{v}^+$	nondimensional velocity field
$\mathbf{v}_s$	velocity field at the free surface
W	work done per unit time per unit width
We	Weber number
w_s	spanwise component of velocity at the free surface
x, y, z	spatial coordinates
$\bar{x}$, $\bar{y}$, $\bar{z}$	nondimensional spatial coordinates
x^+, y^+, z^+	nondimensional spatial coordinates
y_{fs}^+	nondimensional free surface location

Greek symbols

α	thermal diffusivity
α_{surf}	surfactant diffusivity
β	ratio of Marangoni to Weber number
β_L	surfactant–turbulence interaction parameter
γ	surfactant concentration
$\bar{\gamma}$	nondimensional surfactant concentration
γ_0	equilibrium surfactant concentration
δ_{th}	thermal boundary layer thickness
δy^+	nondimensional distance from free surface
Θ	temperature
Θ^*	nondimensional temperature
Θ^{**}	nondimensional temperature
Θ_b	temperature at bottom of computational domain
Θ_{bulk}	bulk temperature
Θ_s	average surface temperature
Θ_s^*	nondimensional average surface temperature
λ	Taylor microscale
ν	kinematic viscosity
π	dynamic pressure
ρ	density
σ	surface tension
$\bar{\sigma}$	nondimensional surface tension
σ_0	equilibrium surface tension
τ_{surf}	shear at the free surface
$\mathbf{\Omega}$	vorticity
$\mathbf{\Omega}^+$	nondimensional vorticity
Ω_x, Ω_y, Ω_z	components of vorticity
Ω_x^+, Ω_y^+, Ω_z^+	nondimensional components of vorticity

interface, should *decrease* the surface temperature. Because of these competing effects it is not clear a priori whether, for example, a naturally occurring surfactant feature on the ocean surface, commonly known as a surface slick, will appear warmer or cooler in infrared images.

The experiments cited above [5,6], along with other recent experiments in a wind wave tank [11] which have exploited infrared technology to determine the relationship between the free surface temperature field and the subsurface velocity field, are also a motivation for our work. These infrared focal plane array technologies allow the determination of the surface temperature field with great thermal, spatial, and temporal resolution. In this context, we wish to consider the circumstances under which surfactant contamination can cause a detectable change in surface temperature. It should be noted that using the currently available sensors, surface temperature changes well below 1 K can easily be detected. In remote sensing applications, such temperature changes may be an indicator of surface slicks of both natural and human origin. Other related reasons

for undertaking this work are given in greater detail in Handler et al. [12].

Surfactants impart an elasticity to the free surface which in turn allows the surface to maintain shear stresses. As a result, turbulent eddies which interact with a contaminated surface will tend to be dissipated by the viscous boundary layer formed by the resistance offered by the interface. This interaction may also significantly change the thermal or mass boundary layers in the region slightly below the surface. Thus, we are interested here in characterizing the degree of surface elasticity necessary to impact the subsurface turbulence.

In previous work [12,13] we have used an open channel turbulent flow to investigate transport processes at free surfaces at low Reynolds numbers and essentially zero Froude number (i.e. no surface deformations). This flow is convenient for these investigations since the turbulence which ultimately impinges upon the surface is generated naturally by mean shear–Reynolds stress interactions acting near the bottom wall. For these and other reasons discussed in [12], we have used open channel turbulence in the work described below.

2. Numerical simulations

2.1. Problem formulation

To explore these issues, a series of direct numerical simulations of open channel flow driven by a constant driving pressure gradient were performed in which several simplifying assumptions were made. First, the *free surface* in these simulations is actually an interface in which no deformations are allowed. Estimates of the surface deformations for the strength of the flows considered here [13] indicate that they are negligible so that a flat boundary model is entirely appropriate. Secondly, buoyancy effects were neglected. For simplicity, however, the passive scalar will be referred to as the *temperature* field.

Given these simplifying assumptions, the equations of motion are solved in dimensionless form by choosing a length scale D, where D is the vertical extent of the channel, and a velocity scale based on the pressure gradient, $u^* = \sqrt{|f|D/\rho}$, where f is a constant pressure gradient, and ρ is the density. The time scale is chosen to be $t^* = D/u^*$. Given these scales the equations of motion in rotational form are given by:

$$\frac{\partial \mathbf{v}^+}{\partial \bar{t}} = \mathbf{v}^+ \times \mathbf{\Omega}^+ - \nabla \pi + \frac{1}{R^*}\nabla^2 \mathbf{v}^+ + 1\hat{\mathbf{e}}_x \tag{2.1.1}$$

and

$$\nabla \cdot \mathbf{v}^+ = 0. \tag{2.1.2}$$

Here, the coordinates in the streamwise, wall normal, and spanwise directions are given respectively by $(\bar{x}, \bar{y}, \bar{z}) = (x/D, y/D, z/D)$, and the corresponding velocity field is given by $\mathbf{v}^+ = \mathbf{v}/u^* = (u^+, v^+, w^+)$. In addition, $\bar{t} = t/t^*$, where t is the dimensional time, so that $\mathbf{\Omega}^+ = \mathbf{\Omega} t^*$, where $\mathbf{\Omega} = (\Omega_x, \Omega_y, \Omega_z)$ is the dimensional vorticity, $R^* = (u^* D)/\nu$, where ν is the kinematic viscosity, and $\pi = (p/\rho + \frac{1}{2}(\mathbf{v}\cdot\mathbf{v}))/u^{*2}$, where p is the pressure, and $\hat{\mathbf{e}}_x$ is a unit vector in the streamwise direction. In the following, an overbar will refer either to the averaging operation or to a nondimensional quantity depending on the context. The computational domain is shown in Fig. 1. In the following, $\bar{y} = 1$ and $\bar{y} = 0$ designate the coordinates for the free surface and the no-slip boundary respectively.

The boundary conditions which are applied at $\bar{y} = 1$ are those for a surfactant contaminated surface with no surface deformation and are given by [4,14]:

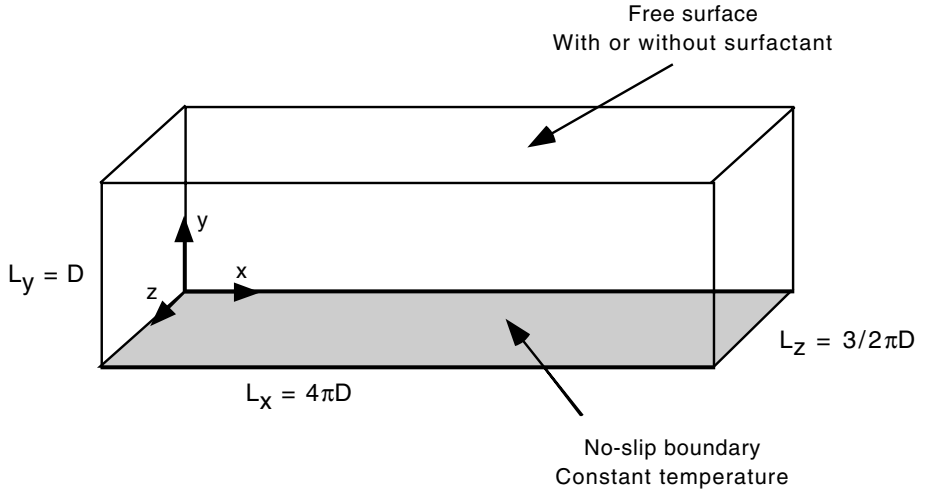

Fig. 1. Computational geometry and coordinate system. Flow is from left to right.

$$v^+ = 0, \tag{2.1.3}$$

$$-\frac{1}{R^*}\frac{\partial u^+}{\partial \bar{y}} + \frac{1}{We}\frac{\partial \bar{\sigma}}{\partial \bar{x}} = 0, \tag{2.1.4}$$

$$-\frac{1}{R^*}\frac{\partial w^+}{\partial \bar{y}} + \frac{1}{We}\frac{\partial \bar{\sigma}}{\partial \bar{z}} = 0, \tag{2.1.5}$$

where (2.1.3) expresses the zero deformation condition, and (2.1.4)–(2.1.5) describe the tangential stress balance at the interface. Here, *We* is the Weber number given by, $We = (\rho u^{*2} D)/\sigma_0$, where $\bar{\sigma} = \sigma/\sigma_0$ and σ and σ_0 are the surface tension and its the equilibrium value respectively. The constitutive model for the surfactant is given by a linearized model [4,14,15]:

$$\bar{\sigma} = Ma(1 - \bar{\gamma}) + 1, \tag{2.1.6}$$

where $\bar{\gamma}$ is the surfactant concentration, γ, made nondimensional by the equilibrium concentration γ_0, and $Ma = -(\mathrm{d}\bar{\sigma}/\mathrm{d}\bar{\gamma})|_0$ is the Marangoni number, where the subscript 0 signifies evaluation at equilibrium.

Note that with this definition, the Marangoni number will be positive for all typical surfactant materials. The advection diffusion equation for an insoluble surfactant is used in these simulations and is given by:

$$\frac{\partial \bar{\gamma}}{\partial \bar{t}} + \nabla_s \cdot (\mathbf{v}_s^+ \bar{\gamma}) = \frac{1}{Pe}\nabla_s^2 \bar{\gamma}, \tag{2.1.7}$$

where $\mathbf{v}_s^+ = u_s^+ \hat{\mathbf{e}}_x + w_s^+ \hat{\mathbf{e}}_z$, $Pe = (u^* D)/\alpha_{\mathrm{surf}}$ is the Peclet number for the surfactant, α_{surf} is the surfactant diffusivity, $\nabla_s = \partial/\partial\bar{x}\hat{\mathbf{e}}_x + \partial/\partial\bar{z}\hat{\mathbf{e}}_z$, $\nabla_s^2 = \partial^2/\partial\bar{x}^2 + \partial^2/\partial\bar{z}^2$, and the subscript 's' associated with a velocity component refers to evaluation at the free surface. We note that setting $Ma = 0$ in (2.1.6) results in the shear free boundary conditions $\partial u^+/\partial\bar{y} = 0$, and $\partial w^+/\partial\bar{y} = 0$ at $\bar{y} = 1$.

Along with the equations of motion, the nondimensional convective-diffusion equation is solved for the temperature field and is given by:

$$\frac{\partial \Theta^*}{\partial \bar{t}} + \mathbf{v}^+ \cdot \nabla\Theta^* = \frac{1}{R^* Pr}\nabla^2\Theta^*, \tag{2.1.8}$$

where $Pr = \nu/\alpha$ is the Prandtl number, and α is the thermal diffusivity. The nondimensional temperature is defined as $\Theta^* = [(\Theta - \Theta_b)k]/(q_0 D)$, where Θ is the temperature, k is the thermal conductivity, q_0 is the magnitude of the heat flux directed normal to the interface at $\bar{y} = 1$, and Θ_b is the temperature at the bottom boundary. Our main concern here is the effect of surfactants on subsurface turbulence as opposed to the effects of surfactants on evaporative heat transport. As a result, we assume that the imposition of the surfactant has no effect on the surface heat flux, (e.g. a liquid phase surfactant is used). With this assumption, the boundary conditions on the temperature field are given by:

$$\frac{\partial \Theta^*}{\partial \bar{y}} = -1, \quad \bar{y} = 1, \tag{2.1.9}$$

$$\Theta^* = 0 \quad \bar{y} = 0. \tag{2.1.10}$$

2.2. Choice of nondimensional parameters

Our simulations were chosen to correspond to water flowing in a channel of dimension $D = 5$ cm, so that $\rho = 1\ \mathrm{g\,cm^{-3}}$, $\nu = 0.01\ \mathrm{cm^2\,s^{-1}}$, and $\sigma_0 \approx 72\ \mathrm{dyne\,cm^{-1}}$. We choose $R^* = 180$ so that $u^* = 0.36\ \mathrm{cm\,s^{-1}}$, which then gives $We = 9 \times 10^{-3}$.

In these simulations we change the surface elasticity by varying *Ma* while keeping the Weber number constant. It is significant to note, however, that for real surfactants $A = -(\mathrm{d}\sigma/\mathrm{d}\gamma)|_0$ is essentially constant over a wide range of surfactant concentrations. As a result, the Marangoni number ($Ma = A\gamma_0/\sigma_0$) can be changed only by changing γ_0 which in turn changes σ_0. It follows that the Weber number must also change since it depends inversely on σ_0. We conclude that in a physical experiment it is not possible to change *Ma* and *We* independently. However, as we discuss in detail below (Section 4), it is the *ratio* of the Marangoni and Weber number, $\beta = Ma/We = (A\gamma_0)/(\rho u^{*2} D)$, which is of greatest importance in this work. Furthermore, β does not depend on the surface tension so that with A, ρ, u^*, and D fixed, it can be changed by changing the surfactant concentration alone. We also note that $A\gamma_0$, which is sometimes referred to as the elasticity, can be interpreted simply as the surface tension difference between a clean and contaminated surface which acts to oppose fluid motions arising from beneath the free surface. Therefore, although we vary *Ma* with *We* fixed, this is done merely as a numerical convenience since it is understood from the discussion above that β is the parameter of importance. A summary of the parameters in each simulation is given in Table 1.

In addition, we note that the actual Prantdl number in pure water at room temperature is ≈5. Computations for such a large Prandtl number would require a very fine grid resolution to resolve the smallest temperature scales. The required resolution is beyond our current computer resources, although we believe the use of a virtual Prandtl number of 2 for the present study works

Table 1
Simulation parameters

Run	R^*	Pr	Ma	We	Pe	β
1	180	2	10^{-2}	9×10^{-3}	10^3	1.1
2	180	2	10^{-3}	9×10^{-3}	10^3	1.1×10^{-1}
3	180	2	3×10^{-4}	9×10^{-3}	10	3.3×10^{-2}
4	180	2	10^{-4}	9×10^{-3}	10	1.1×10^{-2}
5	180	2	0	9×10^{-3}	–	0

appropriately to simulate turbulent heat transfer processes generated by the largest scales of motion [16].

2.3. Numerical methods

The simulations are carried out using the same procedure outlined in [12] in which a fourth order system is solved for the vertical velocity and a second order system is solved for the vertical vorticity. The other components of velocity are recovered from the imposition of continuity.

With this formulation, a boundary condition in addition to (2.1.3) is required for v^+ at the free surface and can be found using (2.1.2), and (2.1.4)–(2.1.5). This results in:

$$\frac{\partial^2 v^+}{\partial \bar{y}^2} = -\frac{R^*}{We}\nabla_s^2 \bar{\sigma} \quad \bar{y} = 1. \tag{2.3.1}$$

This condition reduces to $\partial^2 v^+/\partial^2 \bar{y} = 0$ at a shear free boundary. At the bottom boundary, $\bar{y} = 0$, we employ no-slip conditions $u^+ = v^+ = w^+ = 0$ and $\partial v^+/\partial \bar{y} = 0$. It should be noted that the boundary condition for the vertical vorticity, Ω_y^+, in the surfactant case is:

$$\frac{\partial \Omega_y^+}{\partial \bar{y}} = 0, \quad \bar{y} = 1, \tag{2.3.2}$$

which would also be valid at a shear free boundary.

The equations of motion (2.1.1)–(2.1.2) and the evolution equation for the surfactant (2.1.7) were solved simultaneously with the heat transfer equation (2.1.8) using a psuedo-spectral approach in which the velocity and temperature fields are expanded in Fourier modes in $\bar{x}$ and $\bar{z}$ and Chebyshev modes in $\bar{y}$. The Courant–Friedrichs–Lewy number, defined in [12] remained below ≈ 0.25 in each simulation. The calculations for the velocity, temperature, and surfactant were fully dealiased in the Fourier directions using the 3/2's rule.

The resolution was $128 \times 129 \times 128$ in the x, y, and z directions respectively and the corresponding domain lengths were $L_x/D = 4\pi$, $L_y/D = 1$ and $L_z/D = 3\pi/2$. If an inner or viscous length scale is defined by $l^+ = \nu/u^*$, then in these units the domain is $2262 \times 180 \times 848$. The corresponding grid resolution in inner units in the x and z directions are 17.7 and 6.6, respectively. Length scales made nondimensional in this way will be denoted with a superscript $+$, such as $x^+ = x/l^+$.

3. Turbulence statistics

The initial conditions for the series of simulations described here were fully converged velocity and temperature fields obtained from our previous work [12]. The surface of the flow was then subject, at $\bar{t} = 0$, to a uniform surfactant concentration field, $\bar{\gamma} = 1$. The velocity, temperature, and surfactant fields were then allowed to evolve until a statistically steady state was achieved before flow realizations were stored for analysis. In each run, the total computational time after the statistically steady state was achieved was roughly 21 large eddy turnover times, where the turnover time is estimated as D/u^*. The results described below were obtained from these flow realizations.

It should be noted in Table 1 that for runs 3 and 4, the Peclet number for the surfactant field was decreased (i.e. increased diffusion) compared with runs 1 and 2. The reason for this is that for the lower Marangoni numbers used in runs 3 and 4 the surfactant field developed unphysical Gibbs oscillations as the surfactants tended to occasionally form sharp fronts. Increased diffusion was needed to eliminate this behavior. In general, it has been our observation that the use of increased diffusion did not affect the qualitative nature of the results. It may perhaps be argued that a better approach would be to introduce, for the equations governing the surfactant, an algorithm such as FCT [17], or perhaps a diffusivity which acts only at higher wavenumbers (i.e. small scales) such as a hyperviscosity. These approaches may be undertaken in future work.

3.1. Velocity and vorticity statistics

In previous work [12] we have compared a wide range of near wall statistics to previously established results and have found favorable agreement. In fact the results for the so-called *clean* surface which we present below were obtained from those previous results. In Table 1, the parameter of special concern is the Marangoni number, which was varied from zero (no surface elasticity) to as high as 10^{-2}. In the latter case it will be shown that the surface is highly contaminated, as will become evident by the significant changes observed in the underlying turbulence. For purposes of brevity, we will refer to the $Ma = 0$ case as the clean case, and the $Ma = 10^{-2}$ case as the HC (highly contaminated) case.

Before proceeding to examine the details of the statistics, it is important to emphasize that because of the strong anisotropy of the turbulence in the present case, some statistics will be more greatly affected by the imposition of surfactants than others. As a result, for statistics which are only weakly affected by surfactants, it may be difficult to separate out the effects of the surfactant from random errors associated with the finite number of realizations used to compute these statistics. Nevertheless, in most cases, the effects of surfactants near the free surface are sufficiently strong so that their effects on the statistics can easily be discerned. We expect the effects of surfactants to be important only in the vicinity (on the order of the Taylor microscale) of the

free surface. Nevertheless, the statistics show some apparent differences between surfactant and nonsurfactant cases well away from the free surface. We attribute these differences primarily to finite sample size effects, although surfactants do appear to have an effect on some quantities far from the free surface. To separate out the physical effects of surfactants unambiguously from sample size effects throughout the depth of the channel would require a prohibitively large sample size and a concomitantly large increase in computational effort, and is therefore beyond the scope of the present work.

The mean velocity profiles, $U^+ = \overline{u^+}$, are shown in Fig. 2. It is evident that the surfactant does not affect the region of logarithmic behavior which exists for each value of the Marangoni number. It is interesting to note, however, that the average streamwise velocity at the free surface in the HC case is about 4% larger than in the clean case. In Fig. 2, and in some other figures shown below, we have included inserts which are closeup views of the results in the region $140 < y^+ < 180$ so that greater detail can be discerned in the vicinity of the free surface.

In the discussion to follow, a primed quantity will denote a time dependent one for which the mean has been removed (e.g. u' is the fluctuating streamwise velocity) and u_{rms} will denote a root mean square (rms) value. In Figs. 3–5, the rms profiles for the three components of velocity are given. It is clear that in the near surface region, roughly $160 < y^+ < 180$, that the effect of surface elasticity is to reduce the rms levels for each velocity component. In addition, as the surface condition varies from clean to HC, the turbulence intensities decrease in a consistent and monotonic manner.

It is evident that for the clean case, the rms levels for the tangential components of velocity actually *increase* as the free surface is approached. Thus there is effectively a local maximum for u_{rms} and w_{rms} at the free surface. This behavior, which has been observed in experiments [18] and in simulations [12,13,16,19–21] appears to be a result of the redistribution of turbulent kinetic energy during so-called *splatting* (upwelling) events. During such an event (described in [12]), hairpin-like eddies which originate in the near wall region advect upward. The flow between the legs of a typical hairpin (see Figs. 18 and 19 in [12]) forms a vertical jet which impinges upon the free surface. The vertical kinetic energy is then redistributed to the horizontal components of velocity giving rise to the local maxima in their rms values at the surface as noted above. It is evident from the results shown in Figs. 3 and 5 that the effect of surfactants is to eliminate these local surface maxima. The most striking example of this can be seen in the w_{rms} profile. Here it can be seen that adding a small elasticity to the surface ($Ma = 10^{-4}$) has changed the location of the local maximum from the surface to slightly below it. For the HC case, the local maximum has completely disappeared and the magnitude of w_{rms} at the surface has been greatly reduced relative to its value for the clean case.

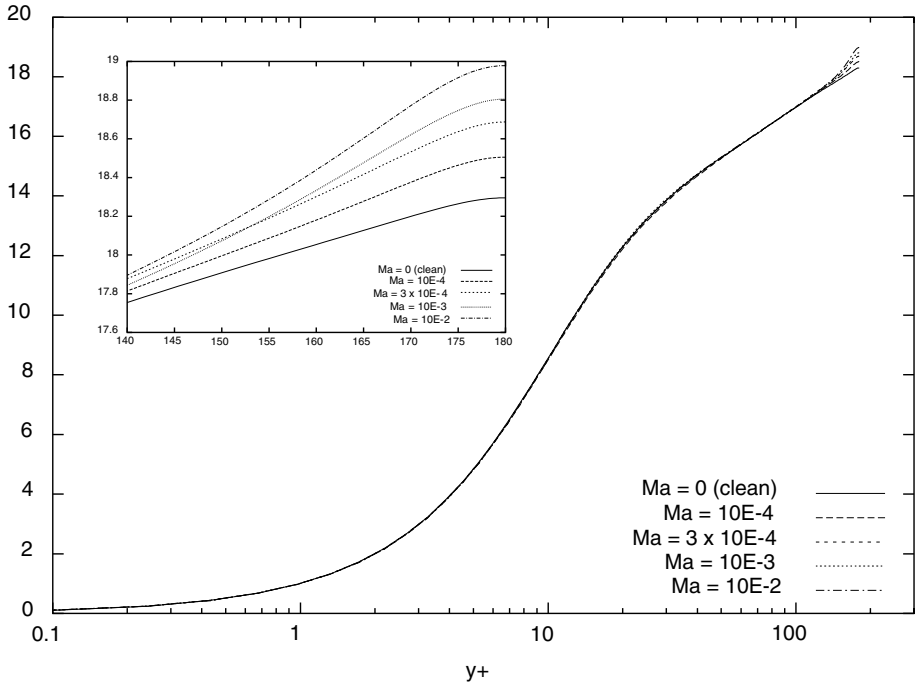

Fig. 2. Dependence of the mean velocity profile on surface elasticity.

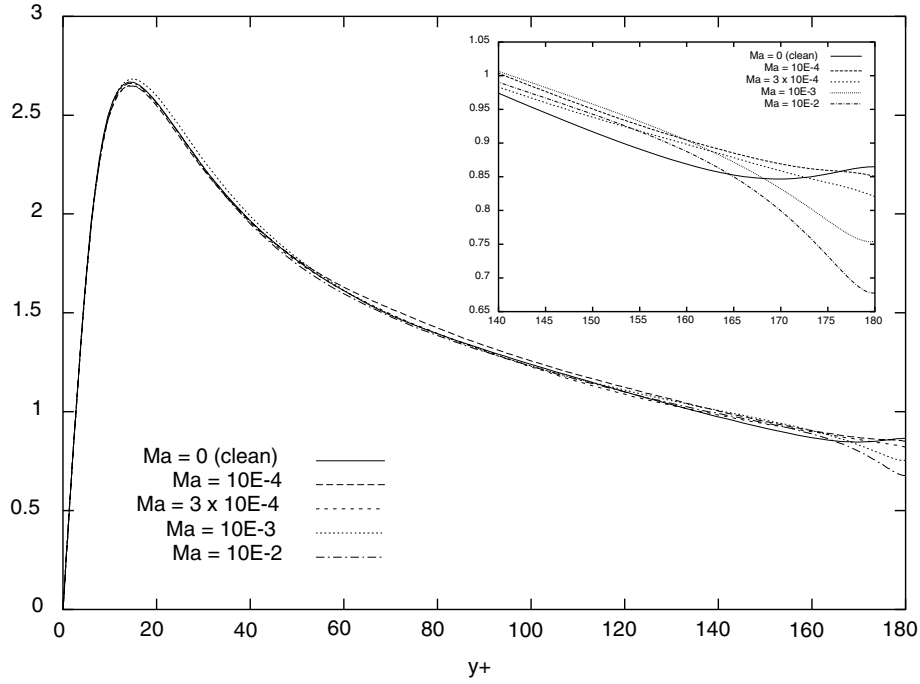

Fig. 3. Dependence of the rms streamwise velocity on surface elasticity. Velocity is normalized by the friction velocity (u^*).

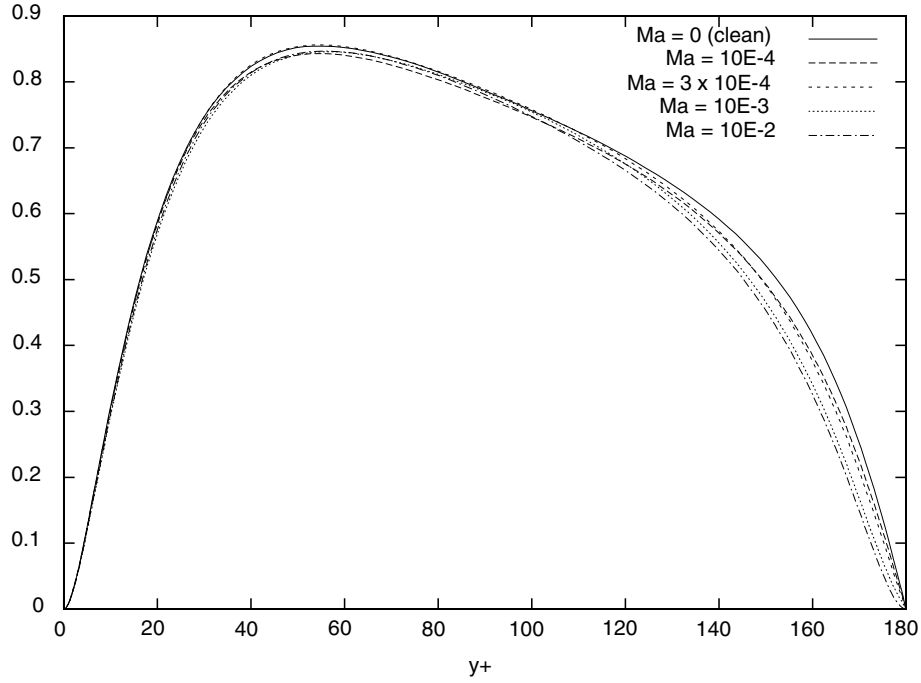

Fig. 4. Dependence of the rms vertical velocity on surface elasticity. Velocity is normalized by the friction velocity.

Given the scenario described above in which hairpin eddies are the principal coherent structure giving rise to surface renewal, it is possible to understand these results in a heuristic manner. We first note from Figs. 3–5 that

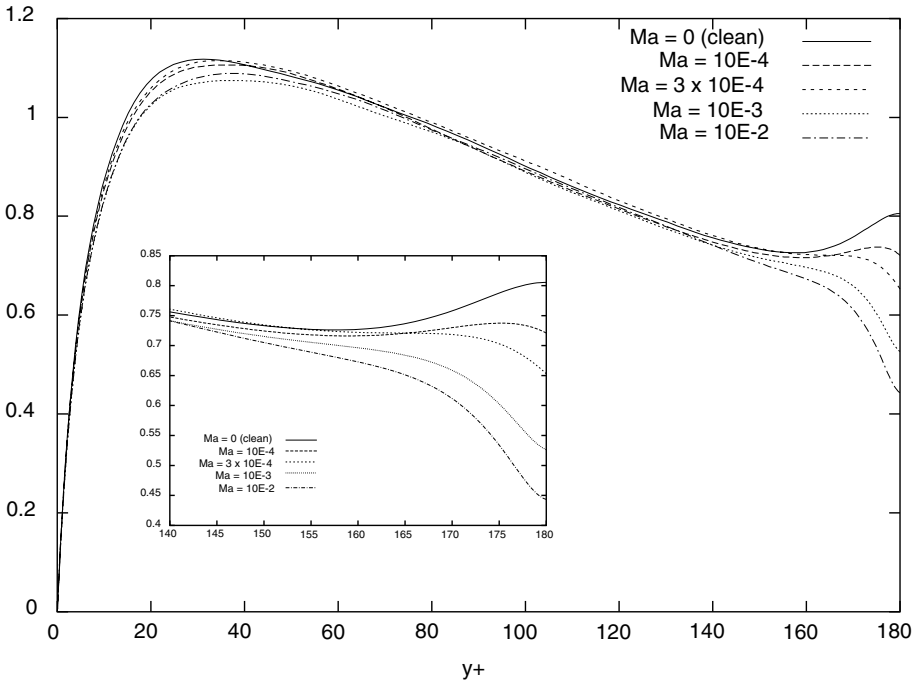

Fig. 5. Dependence of the rms spanwise velocity on surface elasticity. Velocity is normalized by the friction velocity.

the presence of surfactants at the free surface appears to have little or no effect on the turbulent statistics in the near wall region ($30 > y^+ > 0$). As a result, it is easy to surmise that the hairpin-like eddies which are generated there begin their lifetimes with equal strength whether or not surfactants are present. As a typical hairpin encounters a surfactant covered interface, we can envision that at the center of the hairpin the surfactant material should be swept toward the outer edges of the vortex system and should accumulate there. The resultant surfactant concentration gradients lead immediately to a surface shear (see Eqs. (2.1.4)–(2.1.5)) in a direction opposite to the near surface flow, thereby retarding the horizontal (u and w) fluid motions, the retardation being quite evident in Figs. 3 and 5. In accordance with this description, we would thereby expect an increase in viscous dissipation in the near free surface region.

It is important to note that although the effect of the surfactant is to significantly decrease the horizontal components at the boundary, we cannot expect, even in the limit of very high surface elasticty, that the surface turbulence will approach that of a no-slip boundary. The principal reason for this is that although the surfactant will support *fluctuations* in surface shear, no mean shear can be supported. This is evident by taking the horizontal average ($\langle\rangle = (1/(L_x/D)(L_z/D)) \int \mathrm{d}\bar{x}\mathrm{d}\bar{z}$) of equations Eqs. (2.1.4)–(2.1.5) yielding:

$$\frac{\partial\langle u^+\rangle}{\partial\bar{y}} = \frac{\partial\langle w^+\rangle}{\partial\bar{y}} = 0, \tag{3.1.1}$$

which is valid at any instant in time. As a result, just as in the case of a shear free boundary, there can be no mean turbulence production at a surfactant contaminated boundary. Since the existence of a mean shear appears to be a necessary ingredient for the generation of near wall streamwise vortices [22,23] we therefore cannot expect such structures no matter how high the surfactant contamination. On the other hand, the significant damping of the turbulence may give rise to some charateristics of near (no-slip) wall behavior. We might expect the character of the turbulence in this case to be in some sense intermediate between that of a no-slip and a shear free boundary.

We note in Fig. 4 that surfactants also significantly damp the vertical velocity fluctuations in the vicinity of the free surface. In particular, it is of some interest to examine the near free surface asymptotic behavior for the vertical fluctuations. These expansions are given below for the case of a no-slip boundary, shear free boundary, and a surfactant contaminated boundary respectively as follows:

$$v^{+\prime} = c_{\mathrm{ns}}\delta y^{+^2} + d_{\mathrm{ns}}\delta y^{+^3} + \mathrm{O}(\delta y^{+^4}), \tag{3.1.2}$$

$$v^{+\prime} = b_{\mathrm{sf}}\delta y^{+} + d_{\mathrm{sf}}\delta y^{+^3} + \mathrm{O}(\delta y^{+^4}), \tag{3.1.3}$$

$$v^{+\prime} = b_{\mathrm{surf}}\delta y^{+} + c_{\mathrm{surf}}\delta y^{+^2} + \mathrm{O}(\delta y^{+^3}), \tag{3.1.4}$$

where $\delta y^{+} = y^{+} - y^{+}_{\mathrm{fs}}$ and y^{+}_{fs} defines the location of the free surface. It is clear that to leading order, the asymptotic nature of $v^{+\prime}$ for the surfactant case and the shear free boundary case are identical. This is essentially confirmed in Fig. 6, which is a greatly expanded view of v^{+}_{rms} very near the surface ($179 < y^{+} < 180$), in that $v^{+}_{\mathrm{rms}} \approx \delta y^{+} + \cdots$ for $Ma = 0$–10^{-3}. On the other hand, for $Ma = 10^{-2}$ v^{+}_{rms} appears to deviate somewhat from linear behavior. This is confirmed by noting that $|(\partial^2 v^{+}/\partial\bar{y}^2)/(\partial v^{+}/\partial\bar{y})| \simeq 5$ near the free surface for the $Ma = 0$–10^{-3} cases, whereas for $Ma = 10^{-2}$ this ratio is of order 500. This corresponds to the clear curvature indicated in the v^{+}_{rms} profile for $Ma = 10^{-2}$. Thus the presence of high surface elasticity has changed the asymptotic behavior of the vertical velocity fluctuations to more nearly approach that found near a solid boundary. In Fig. 7 we note that the reduced vertical and streamwise velocity fluctuations in the surfactant cases have also resulted in a reduced Reynolds stress near the free surface.

The components of vorticity in the x, y, and z directions are given respectively by:

$$\Omega^{+}_{x} = \frac{\partial w^{+}}{\partial\bar{y}} - \frac{\partial v^{+}}{\partial\bar{z}}, \tag{3.1.5}$$

$$\Omega^{+}_{y} = \frac{\partial u^{+}}{\partial\bar{z}} - \frac{\partial w^{+}}{\partial\bar{x}}, \tag{3.1.6}$$

$$\Omega^{+}_{z} = \frac{\partial v^{+}}{\partial\bar{x}} - \frac{\partial u^{+}}{\partial\bar{y}} \tag{3.1.7}$$

and their rms profiles are shown in Figs. 8–10. It is evident from these definitions that in the absence of vertical shear at the free surface ($\partial w^{+}/\partial\bar{y} = \partial u^{+}/\partial\bar{y} = 0$) there can be no x or z components of vorticity there, as indicated in Figs. 8 and 10. On the other hand, the y component of vorticity is nonzero at a shear free clean boundary as indicated in Fig. 9. The effect of the addition of surfactants is clearly to increase both the x and z components of the vorticity fluctuations at the surface which can be readily explained by the capacity of surfactants to support a fluctuating surface shear. It is interesting to note that for each of these components (x and z) of vorticity, a local maximum in rms levels occurs at the free surface in the HC case. While the effect of surfactants is to strongly increase Ω^{+}_{x} and Ω^{+}_{z} fluctuations, Ω^{+}_{y} levels appear to decrease only marginally. One possible interpretation for this is that as the hairpin-like vortices impinge upon the surface from below, they *attach* themselves to the surface [24] and create spin in the plane of the surface. This creates (locally) an essentially rigid body rotation with very little surface divergence, where the surface divergence is defined by $S = \nabla_{\mathrm{s}} \cdot \mathbf{v}^{+}_{\mathrm{s}} = -\partial v^{+}/\partial\bar{y}|_{\bar{y}=1}$. As will be shown, regions of strong surface divergence will be closely related to regions of accumulation or depletion of surfactant material. It follows that the surfactant will undergo little compression or expansion after such an event has taken place, leaving the vortices free to spin and thus giving rise to little decrease in vertical vorticity.

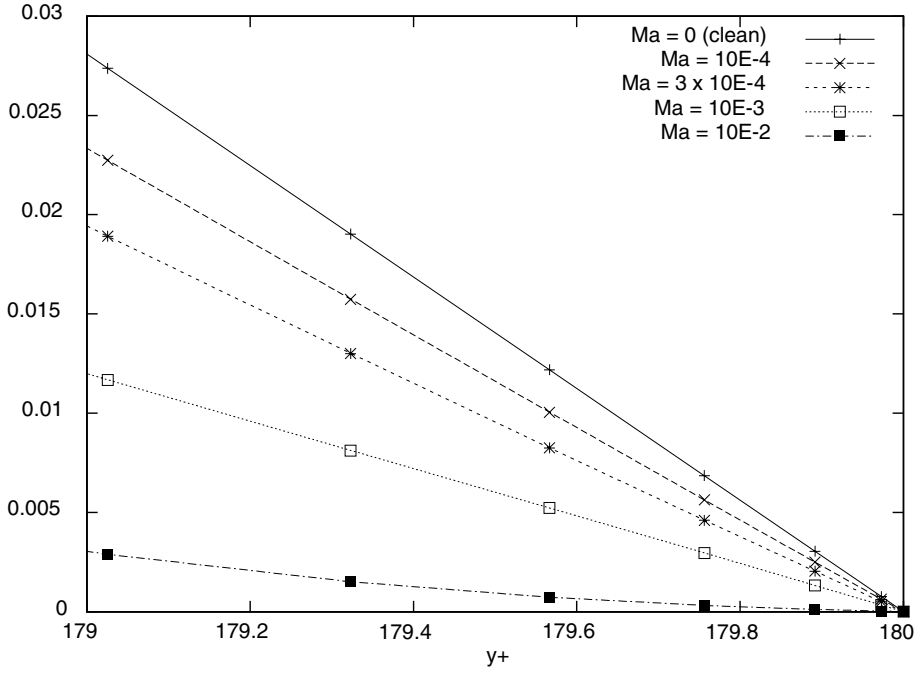

Fig. 6. Closeup view of the rms vertical velocity and its dependence on surface elasticity. Velocity is normalized by the friction velocity.

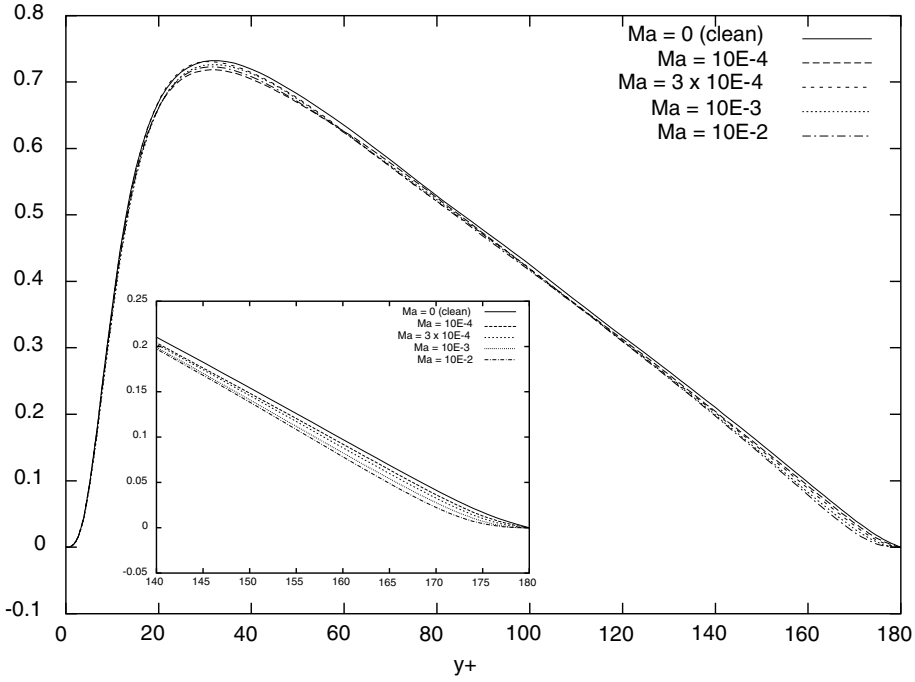

Fig. 7. Dependence of the Reynolds stress, $-\overline{u'v'}/u^{*2}$, on surface elasticity.

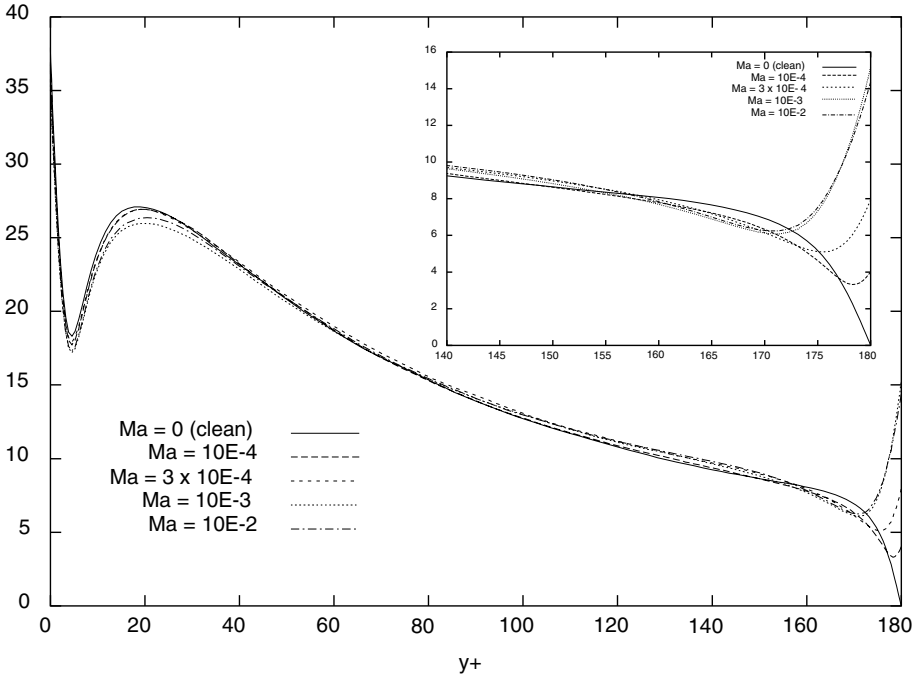

Fig. 8. Dependence of the rms of the streamwise vorticity, $(\Omega_x D)/u^*$, on surface elasticity.

3.2. Temperature and surfactant statistics

In Fig. 11 the mean temperature profiles are shown. It is clear from these results that the surface temperature decreases monotonically with increasing surface elasticity. To understand this we note that a linear expansion of the mean temperature in the vicinity of the free surface yields:

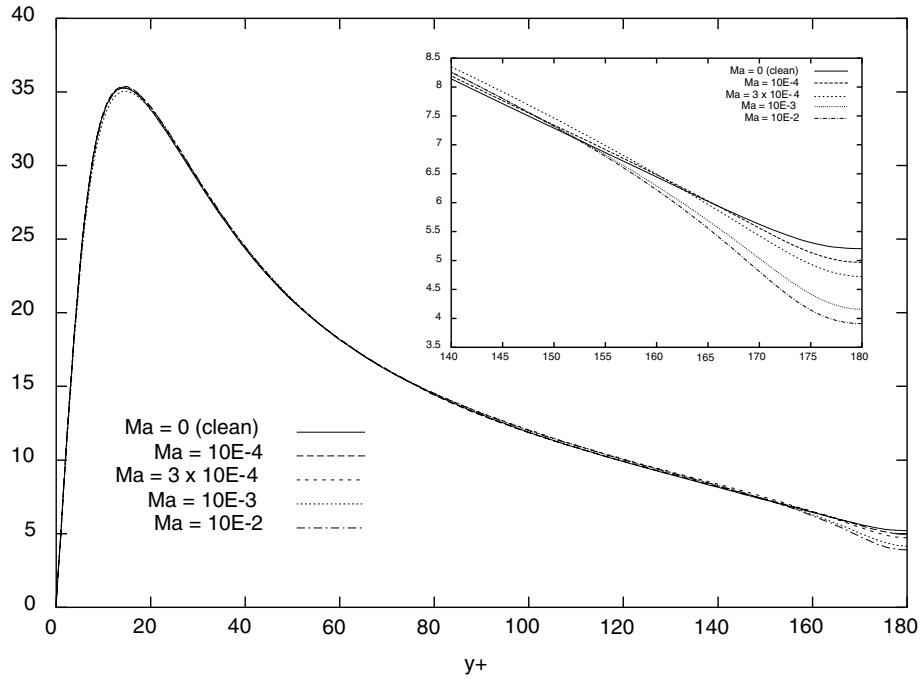

Fig. 9. Dependence of the rms of the vertical vorticity, $(\Omega_y D)/u^*$, on surface elasticity.

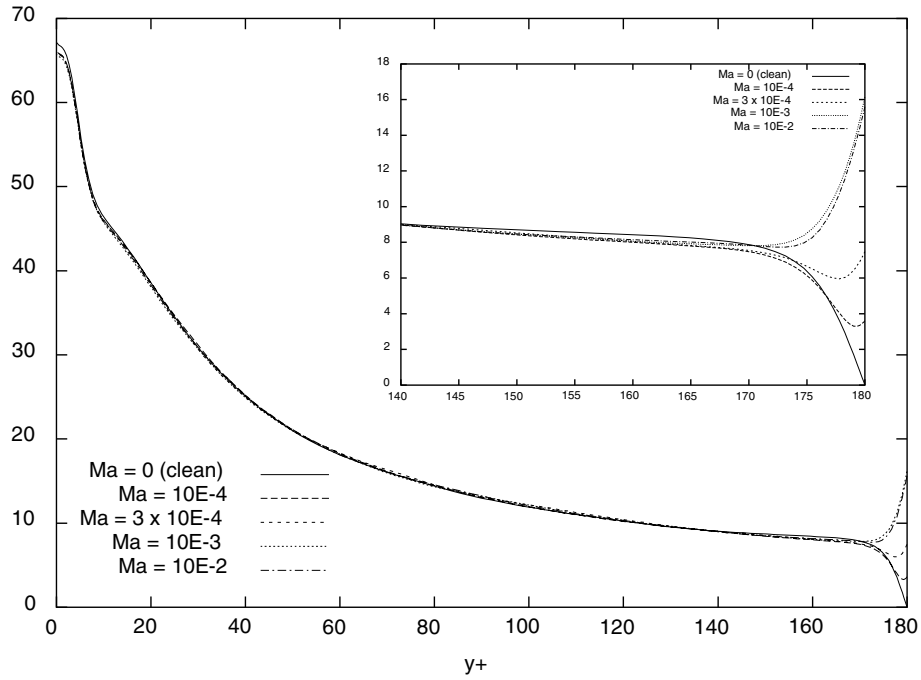

Fig. 10. Dependence of the rms of the spanwise vorticity, $(\Omega_z D)/u^*$, on surface elasticity.

$$(\Theta_s - \Theta_{bulk}) = -(\delta_{th} q_0)/k, \tag{3.2.1}$$

where Θ_s is the mean surface temperature and Θ_{bulk} is a suitably defined mean *bulk* temperature which we define here as the temperature where all the profiles in Fig. 11 appear to converge, and δ_{th} is a nominal thermal boundary layer thickness. This convergence appears at about $y^+ = 140$ where $\Theta_s^* \approx -0.085$. Since the heat flux

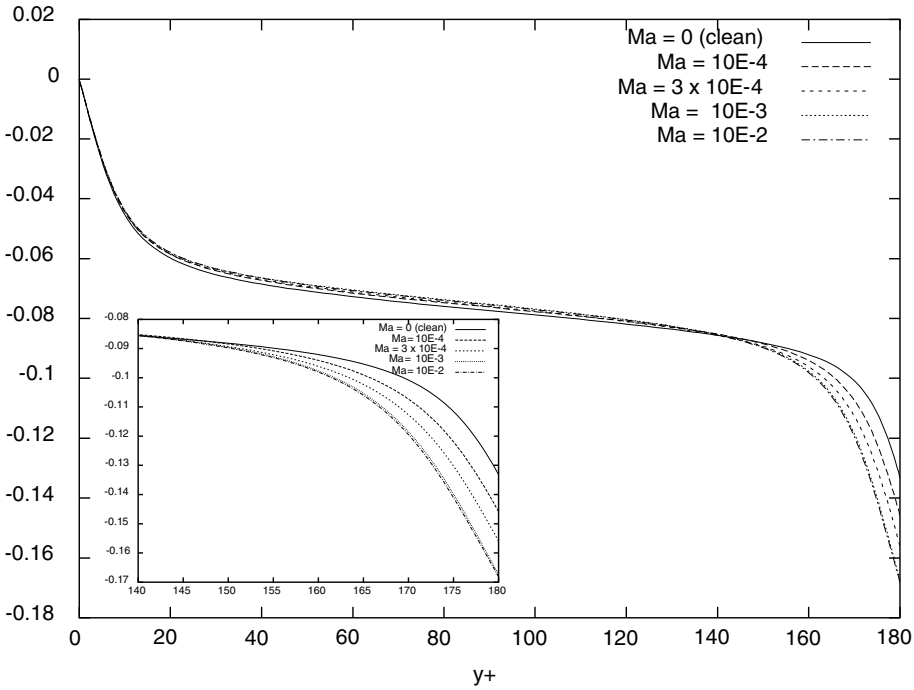

Fig. 11. Dependence of the mean temperature, $\overline{\Theta^*}$, on surface elasticity.

at the interface is assumed to be independent of the surface elasticity in these simulations, (3.2.1) indicates that increases in the thermal boundary layer thickness will correspond to a *decrease* in the surface temperature. In Table 2 we have computed δ_{th}/D and the change in surface temperature in degrees Kelvin relative to the clean case. This temperature change was computed using $q_0 = 100\ \mathrm{W/m^2}$, which is typical of the heat flux found in unforced evaporative cooling in a laboratory setting [25], and $D = 5$ cm. It is evident that although the temperature changes are small (on the order of 0.3 K for the HC case), they are an order of magnitude larger than the thermal resolution (2×10^{-2} K) of currently available infrared detectors [5,6,25] and should therefore be easily detectable. Some confirmation of this result can be found in recent work [5] in which surfactants were clearly found to decrease surface temperatures by about 1 K compared to a clean interface. The cooling of the interface naturally leads to a clear decrease in the Nusselt number ($Nu = (q_0 D)/(k(\Theta_{\mathrm{b}} - \Theta_{\mathrm{s}}))$ as shown in Table 2.

A heuristic, dynamical explanation for the cooling of the surface by surfactants can be obtained by referring to the surface strain model which has been described in considerable detail in several recent works [12,25–27]. According to the model, the steady state thermal boundary layer thickness is ultimately determined by the vertical strain rate, $\partial v/\partial y$, evaluated at the free surface. For example, it is envisioned that during a splatting event, where $\partial v/\partial y < 0$ at the surface, the thermal boundary layer is thinned as it becomes compressed against the free surface. Following the splat, the magnitude of the vertical strain rate decreases and the thermal boundary layer thickens due to molecular diffusion. In the present case, we should expect the surfactant to have essentially no effect on the production of turbulence at the no-slip wall, so that it can be safely assumed that surfactants should have no effect on the frequency of such splatting events. On the other hand, the strength of the typical hairpin vortex, which we assume to be responsible for the typical splat, is clearly reduced by the presence of surfactants as it encounters the surface layer (say one Taylor microscale from the surface). As a result, the vertical strain rate should decrease in the presence of surfactants and we would therefore expect a thicker thermal boundary layer, which we indeed observe. In Fig. 12 a plot of the rms of the vertical strain rate at the free surface versus *Ma* clearly shows this decrease and is therefore quite consistent with this conjecture. It is interesting to note that the vertical strain rate fluctuations decrease only by an order of magnitude as the surface elasticity increases by two orders of magnitude. In Fig. 13 we show that there is also a corresponding decrease in the fluctuations of surfactant concentration with increasing *Ma*. In summary, the effect of surface elasticity as embodied in the surfactant ap-

Table 2
Thermal statistics

Run	Ma	δ_{th}/D	Nu	$\Delta\bar{\theta}^*$	$\Delta\bar{\theta}K$	θ^*_{rms}	θ^{**}_{rms}
1	10^{-2}	0.0812	5.95	−0.035	−0.29	0.0237	0.141
2	10^{-3}	0.0804	5.98	−0.034	−0.28	0.0254	0.152
3	3×10^{-4}	0.0716	6.41	−0.023	−0.19	0.0307	0.197
4	10^{-4}	0.06	6.86	−0.013	−0.11	0.0321	0.220
5	0	0.0471	7.51	0	0	0.0278	0.209

$\Delta\bar{\theta}^*$ is the difference between the mean surface temperature in the clean case and mean surface temperature in any given run. $\Delta\bar{\theta}$ is the same temperature difference based on a heat flux of 100 W/m^2 and the thermal properties of water. $\theta^{**} = (\theta - \theta_b)/(\theta_b - \theta_s)$ as defined in the text. θ^*_{rms} and θ^{**}_{rms} are rms surface temperatures.

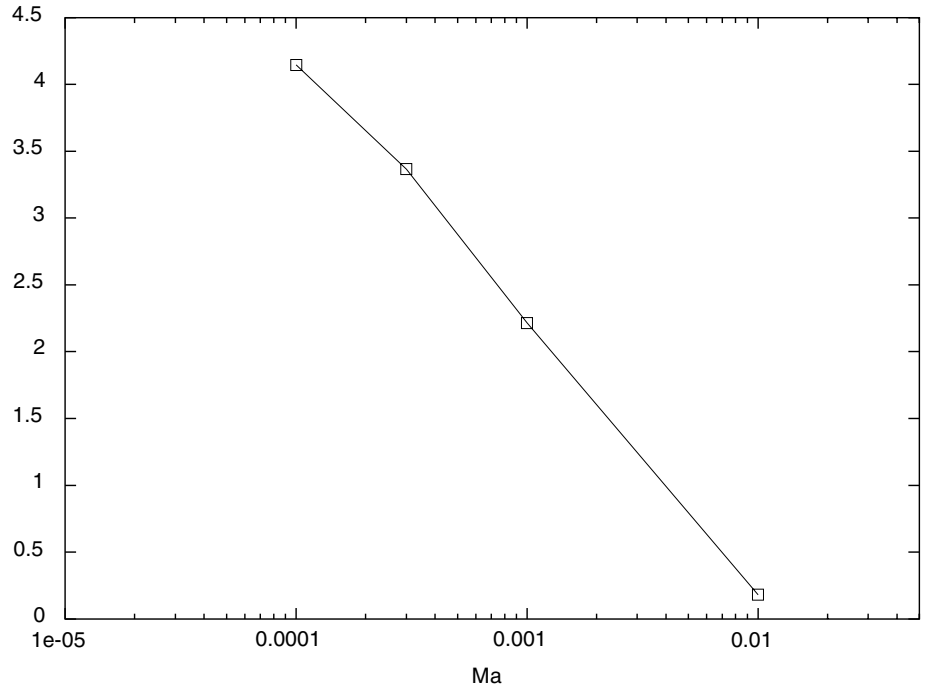

Fig. 12. Dependence of the rms of the surface divergence, $S = -\partial v^+/\partial\bar{y}|_{\bar{y}=1}$, on Marangoni number.

pears to be sufficient to decrease the vertical strain rate, which in turn acts to *increase* the thermal boundary layer thickness and to decrease the surface temperature when the surface flux is fixed.

In Fig. 14 the rms of the temperature fluctuations are shown. Somewhat unexpectedly, the rms levels at the free surface for the cases $Ma = 10^{-4}$ and 3×10^{-4} are actually greater than for the clean case. This contrasts with the velocity fields whose rms levels at the free surface decrease monotonically with increasing surfactant elasticity. This can be explained by assuming that the surface renewal eddies emanating from below retain the temperature associated with the fluid far from the free surface (e.g. the temperature of the bulk). In addition, to first order, we may view the surface rms temperature field as due to the difference between the temperature of these eddies and the mean surface temperature, which clearly *decreases* with increasing surface elasticity as noted above (Fig. 11). As a result we might expect that for the lower Ma cases, the rms surface temperature fluctuations could actually increase compared to the clean case. At higher Ma the severely decreased rms vertical strain rates should give rise to decreased surface temperature fluctuations. Some confirmation for this is given in Table 2 which shows that when the surface rms temperature is scaled to take the mean surface

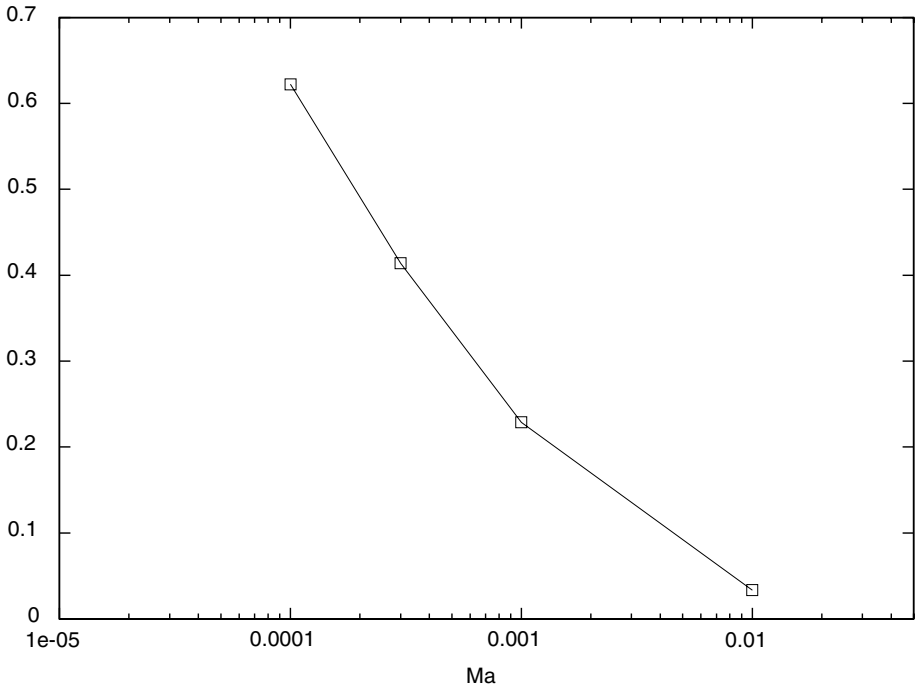

Fig. 13. Dependence of the rms of the surfactant surface concentration, $\bar{\gamma}$, on Marangoni number.

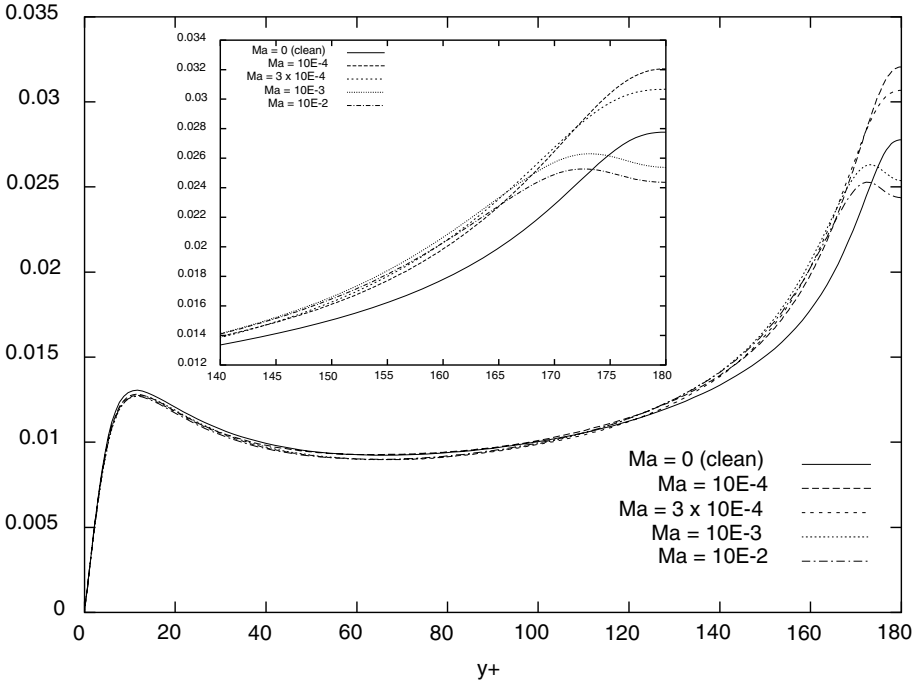

Fig. 14. Dependence of rms temperature, Θ^*, on surface elasticity.

temperature into account (e.g. we use a temperature $\Theta^{**} = (\Theta - \Theta_b)/(\Theta_b - \Theta_s)$), then the surface rms temperature decreases almost monotonically with increased surface elasticity. Finally, Fig. 15 shows that surface

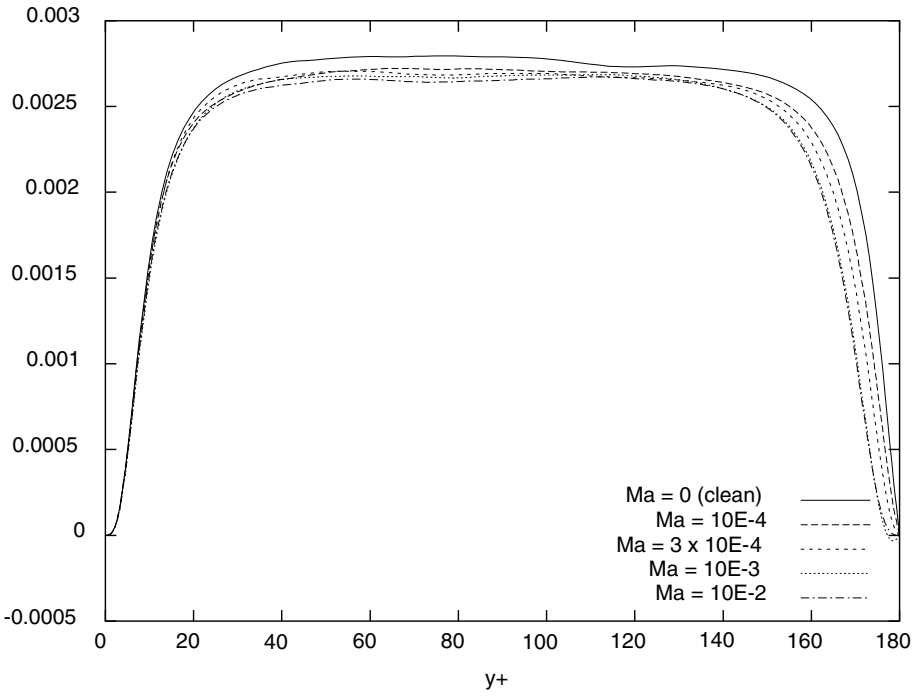

Fig. 15. Dependence of the convective heat flux, $(\overline{\Theta' v'} k)/(q_0 D u^*)$, on the surface elasticity.

elasticity has dramatically decreased the convective heat flux, in particular near the free surface. This is directly reflected in the substantially decreased mean temperatures (Fig. 11) by virtue of the equation for the mean temperature, which can be obtained by performing a Reynolds averaging procedure on (2.1.8).

4. A nondimensional parameter for the characterization of turbulence–surfactant interactions

Examination of the equations of motion and boundary conditions given by Eqs. (2.1.1)–(2.1.6) reveals that if R^* and $\beta = Ma/We$ are fixed, then the flow dynamics must remain unchanged regardless of the values assigned to Ma and We. This simplification would of course not be possible if we allowed for surface deformation. As a result, we must assume that β alone is the parameter controlling the effects of surfactant–turbulence interactions. If we define the surface elasticity [15] as $E = -(\mathrm{d}\sigma/\mathrm{d}\gamma)|_0 \gamma_0$, then $\beta = E/(\rho u^{*2} D)$. This parameter may be viewed simply as a ratio of elastic surface forces to fluid inertial forces, although we develop another interpretation below. In order for β to be useful in describing the physics it should obviously be determined on the basis of *local* velocity and length scales characteristic of the typical eddies in the flow in the vicinity of the surface. We therefore choose a parameter $\beta_L = E/(\rho U_E^2 L_E) = \beta (u^*/U_E)^2 (D/L_E)$, where U_E is the velocity scale associated with a typical energy containing eddy of size L_E.

For the present simulations we have computed β_L (shown in Table 3) by using $L_E/D = (2\lambda)/D \simeq 0.4$ (see [13]), where λ is a typical value of the Taylor microscale near the free surface, and $U_E/u^* \simeq 1$, which is a typical free surface rms velocity. We define the microscale here as $\lambda^2 = 2\overline{v^2}/(\partial v/\partial z)^2$, where v represents any fluctuating velocity component. We have used here a rough average (for the clean case) over all three velocity components of the spanwise (z) microscale. It turns out that this microscale varies little at the free surface with respect to the chosen velocity component.

For comparision purposes, we have also computed β_L (shown in Table 4) for the case of a two dimensional vortex pair interacting with a flat free surface [25]. In this case the flow was obviously much simpler than for the case of fully developed turbulence, although we might think of the vortex pair as mimicking the legs of a hairpin-like vortex as it impacts the free surface. On the other hand, although the vortex pair may be a useful idealization, it must be kept in mind that the two dimensionality of the vortex pair prevents vortex reattachment to the free surface [24] which is allowed in the three dimensional turbulence case. It is evident that for both the turbulence and vortex pair that $\beta_L \simeq 1$ in the most contaminated cases and that in these cases the

Table 3
Surfactant–turbulence interaction parameter for current simulations

Run	β	U_E/u^*	λ/D	β_L
1	1.1	1.0	0.2	2.78
2	1.1×10^{-1}	1.0	0.2	2.78×10^{-1}
3	3.3×10^{-2}	1.0	0.2	8.33×10^{-2}
4	1.1×10^{-2}	1.0	0.2	2.78×10^{-2}
5	0	1.0	0.2	–

U_E is the rms velocity and λ is the Taylor microscale for a typical eddy near the free surface. $\beta_L = E/[\rho U_E^2 L_E]$ is the turbulence–surfactant interaction parameter and $L_E = 2\lambda$.

Table 4
Surfactant–turbulence interaction parameter for vortex ring simulations

Run	β	U_E/u^*	d_E/h	β_L
7	2.78×10^{-3}	0.1	0.4	6.94×10^{-1}
10	2.78×10^{-4}	0.1	0.4	6.94×10^{-2}
11	2.78×10^{-5}	0.1	0.4	6.94×10^{-3}
12	2.78×10^{-6}	0.1	0.4	6.94×10^{-4}

The nature of the various simulations given above as well as the definitions of U_E, the tangential velocity, d_E, the vortex diameter, u^*, and h are given in Ref. [25]. $\beta_L = E/[\rho U_E^2 d_E]$ is the turbulence–surfactant interaction parameter.

effects of surfactants were dramatic. For example, in the turbulence simulations (run 1) there was a strong decrease in w_{rms} and a large drop in surface temperature, and in the vortex pair calculations (run 7), there was a strong rebound of the pair from the contaminated boundary. For $\beta_L \simeq 10^{-3}$ (run 12), the vortex pair exhibited no rebound from the free surface and had a trajectory which was virtually identical to that of a clean surface, and for $\beta_L \simeq 10^{-2}$ (run 11) the pair exhibited a weak rebound, indicating that this was a transitional case between clean and HC. In a similar manner, for $\beta_L \simeq 10^{-2}$ (run 4) in the present simulations, the effects of surfactants were discernable but negligibly small for the full range of turbulence statistics. It is clear that there is a surprisingly good correspondence between the turbulence case and the vortex pair results with regard to the behavior of the near surface flow as a function of β_L, in spite of the aforementioned differences between the two and three dimensional dynamics. As a result, we conclude that for $\beta_L \leqslant 10^{-3}$ the flow will behave essentially as if the surface were uncontaminated. On the other hand, for $\beta_L \geqslant 1$, the flow will be strongly affected by surface elasticity.

It is also possible to interpret β_L, in a heuristic sense, as a ratio of time scales. For this purpose, we can form the two time scales $T_c = L_E/U_E$, and $T_d = (\rho U_E L_E^2)/E$, so that $\beta_L = T_c/T_d$. To interpret these scales, we envision a columnar eddy of effectively infinite length in the z direction, and of diameter L_E with characteristic velocity U_E corresponding to the fluid velocity at the outer edge of the eddy. The scale T_c can then be viewed as the eddy turnover time. When such an eddy encounters a contaminated interface, it loses energy due to the work done it performs to compress the surfactant in the plane of the surface. Referring to (2.1.4–2.1.5), the shear stress generated in this process may be estimated by $\tau_{surf} \simeq E/L_E$ so that the work per unit time per unit width can therefore be estimated as $W = \tau_{surf} L_E U_E \simeq E U_E$. The kinetic energy of the eddy per unit width of the eddy can be estimated as $K = \rho L_E^2 U_E^2$. It follows that $T_d = K/W$, which we interpret as a dissipation time scale in the sense that it gives a rough estimate of time it takes for an eddy of a given kinetic energy to dissipate due to its interaction with an elastic surface. Thus when $\beta_L \simeq 1$ eddies are dissipated quickly, on the order of an eddy turnover time, and we expect the effects of surfactants on the near surface turbulence to be large. On the other hand, $\beta_L \ll 1$ implies that the surface is almost inviscid and the eddies are barely damped, leading to *clean* behavior. Since the simulations show that $\beta_L \leqslant 10^{-3}$ is required to minimize surfactant effects, this implies that a large separation of time scales is needed to render a surface effectively uncontaminated.

5. The structure of the thermal and velocity fields near the free surface

In order to gain some further insight, we display in Figs. 16(a)–(d) and 17(a)–(d) instantaneous horizontal ($x-z$) snapshots (e.g. each image in Fig. 16 was obtained at the same instant of time) of various surface field quantities for the weakly contaminated case ($Ma = 10^{-4}$) and the HC case respectively. In each figure, the mean flow is in the positive x direction, (left to right). In previous work [12] we described in some detail the relation between the surface temperature field and the underlying hydrodynamic field for an uncontaminated interface. This discussion will not be repeated here except to restate a principal conclusion of that work: regions of low streamwise velocity near the surface are closely correlated with upwellings from hairpin-like eddies which are advected from below. This warmer low speed fluid tends to form a wake-like pattern on the surface quite reminiscient of what are termed *fish scales*. The surface temperature and streamwise velocity shown in Fig. 16 are qualitatively the same as in the clean case described in [12]. For example, in the region identified as A in Fig. 16, the patch of warm fluid is well correlated with a region of low streamwise velocity. The surface elasticity in this case is apparently sufficiently small so that upwellings from below can *break through* the surfactant layer and give structures quite similar to the clean case.

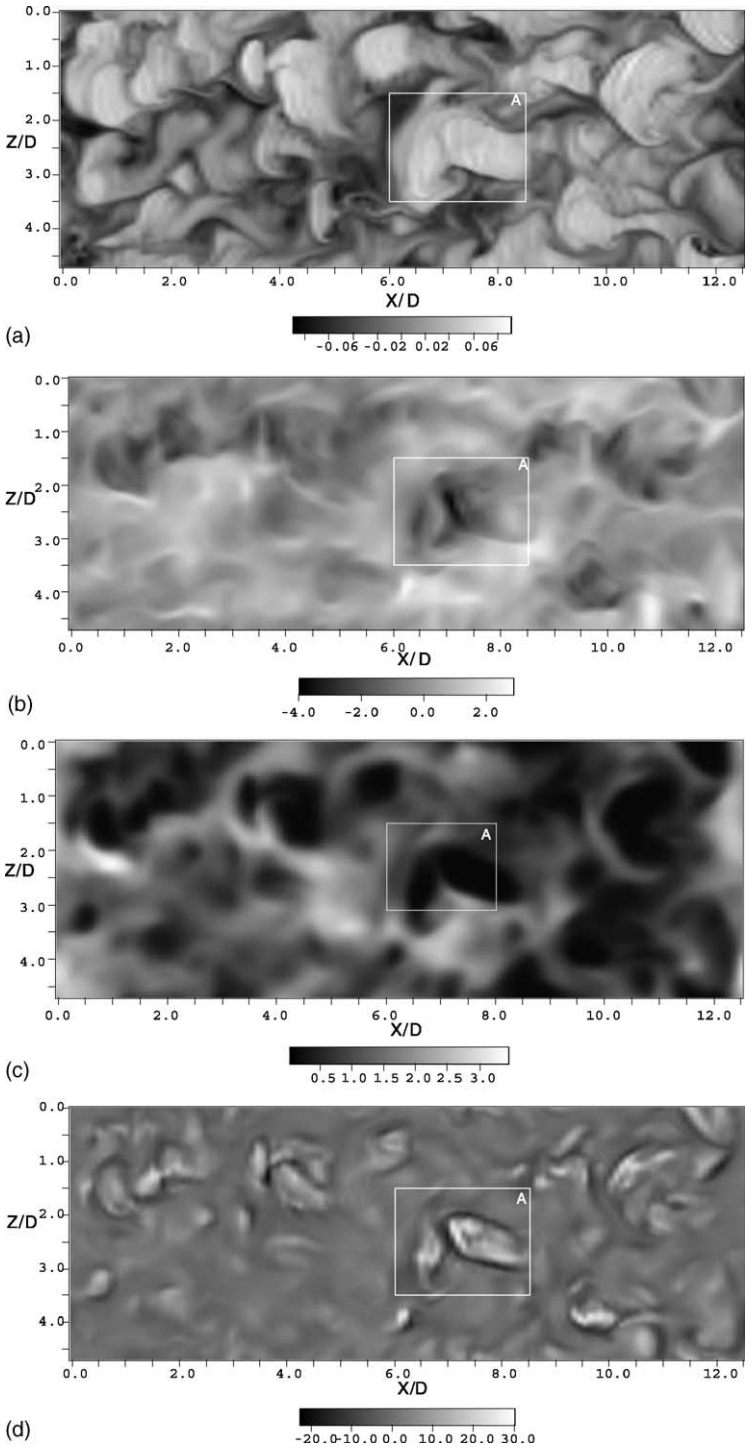

Fig. 16. Instantaneous visualizations at the free surface for $Ma = 10^{-4}$. (a) Fluctuations of the temperature, Θ^*; (b) fluctuations of streamwise velocity, u^+; (c) the surfactant concentration, $\bar{\gamma}$; (d) fluctuations of surface divergence, $-\partial v^+/\partial \bar{y}|_{\bar{y}=1}$.

Before proceeding, we note that (2.1.7) can be re-written (neglecting diffusion):

$$\frac{\partial \bar{\gamma}}{\partial \bar{t}} + \mathbf{v}_s^+ \cdot \nabla_s \bar{\gamma} = -\bar{\gamma} S, \tag{5.1}$$

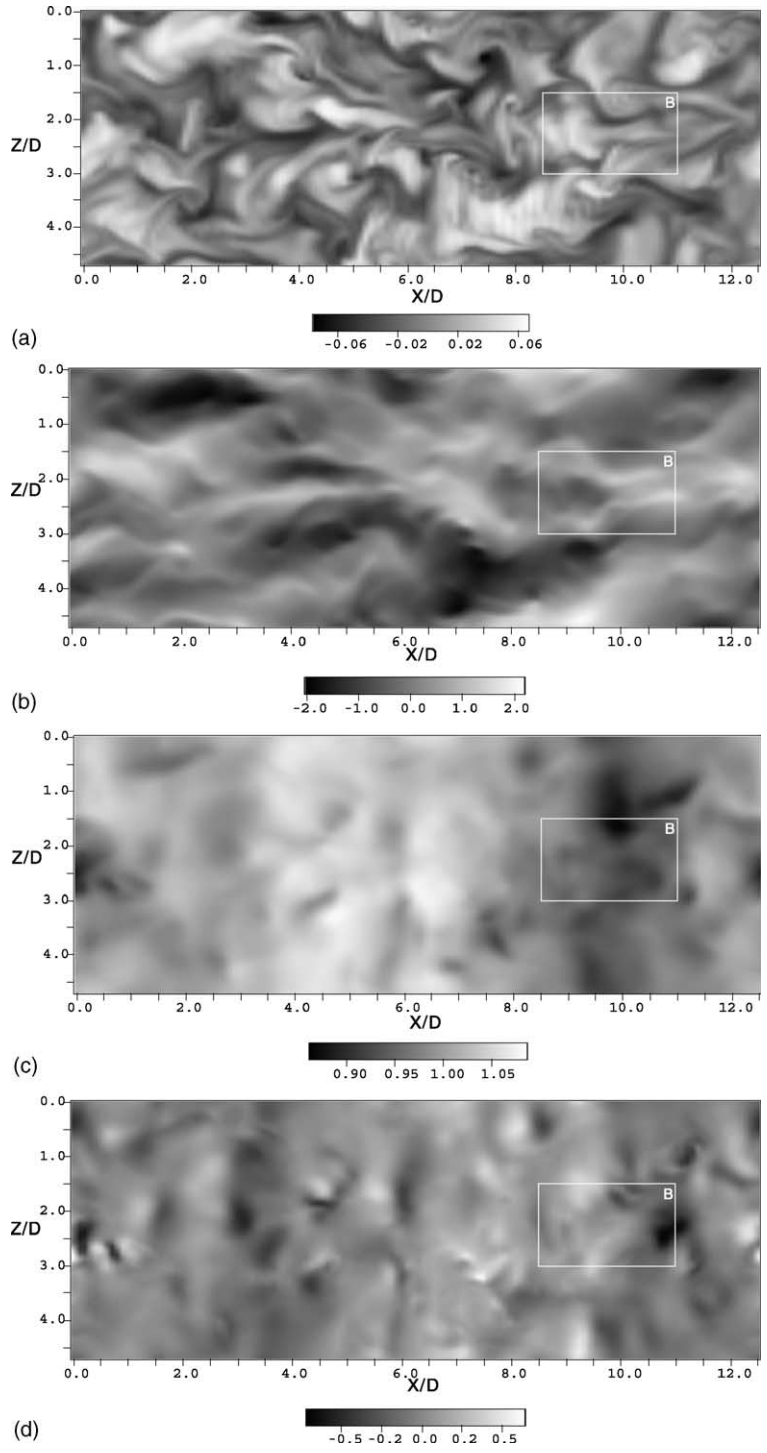

Fig. 17. Instantaneous visualizations at the free surface for $Ma = 10^{-2}$. (a) Fluctuations of the temperature, Θ^*; (b) fluctuations of streamwise velocity, u^+; (c) the surfactant concentration, $\bar{\gamma}$; (d) fluctuations of surface divergence, $-\partial v^+/\partial \bar{y}|_{\bar{y}=1}$.

where $S = -\partial v^+/\partial \bar{y}|_{\bar{y}=1}$ is the surface divergence as noted earlier. Since $\bar{\gamma}$ is always positive, these relations clearly show that the surface divergence acts as a source term for surfactant concentration is such a way that in

regions where $S < 0$ we can expect surfactant to accumulate and conversely when $S > 0$ surfactant material should be removed.

It is evident from Fig. 16(c) and (d) that there is a close correlation between S and the surfactant concentration. In region A, for example, there is relatively large patch for which $S > 0$ which corresponds clearly with a region of very low surfactant concentration. This region of positive surface divergence must also be one in which the vertical strain rate is negative, which would betypical of a splatting event. This type of event appears to be the most prominent appearing in the surface concentration and surface divergence fields, at least in the case in which the surface elasticity is small. We note that in this case, the excursions in the surface concentration are large, ranging from O(0) to greater than 3, and the corresponding surface divergence fluctuations are also large, ranging from O(−20) to greater than 20.

The structure of the surface fields in the HC case is shown in Fig. 17. The correspondence between the low streamwise velocity regions and warm spots in the surface temperature field are evident just as they are in Fig. 16. In particular we have highlighted a region labeled B which contains within it a mushroom shaped high temperature patch which is correlated with a low speed region in Fig. 17(b). An interesting aspect shown in Fig. 17(b) is the apparent existence of a streaky structure in the streamwise velocity field. This structure, although not nearly as prominent as that found in the near wall region of a turbulent boundary layer, may nevertheless indicate some local formation of coherent structures. Since it is well known that such structures are dependent on the existence of a mean shear, which is clearly absent in this case, the appearance of such structures in the surfactant case seems unlikely. On the other hand, surfactants can support a substantially large fluctuating shear, as evidenced by the large magnitude of the rms value of the spanwise vorticity at the free surface in the HC case shown in Fig. 10, so that the production of local shear flow instabilities in the HC cannot be ruled out. In Fig. 17(c) and (d) the surfactant concentration and the surface divergence are shown. It is clear that the fluctuations in both are strongly reduced compared to the nearly clean case. This is certainly to be expected since the high elasticity of the surfactant should strongly damp upwelling events.

6. Summary and conclusions

A series of simulations of statistically steady open channel turbulence were performed in which the effects of surfactants were studied. As the surfactant elasticity was increased, the turbulence intensities were significantly decreased near the free surface. Particularly strong decreases were found in the spanwise velocity fluctuations. All three components of the vorticity were affected by the surfactant, with significant increases found in the horizontal ($x - z$) components of vorticity caused by the ability of surfactants to sustain significant fluctuating surface shear stresses. The presence of surfactants was found also to decrease the average temperature at the free surface. This can be understood by observing that splats tend to thin the thermal boundary layer in competition with thermal diffusion which tends to thicken it. Since surfactants decrease the intensity of the splats, the vertical strain rate is correspondingly reduced, giving rise to a thicker thermal boundary layer. The decrease in the mean surface temperature was found to be about 0.3 K lower in the case of high surface contamination compared to a clean surface. This result corresponds reasonably well with recent experimental studies in which high resolution IR sensors have been employed. In addition, the temperature fluctuations, appropriately normalized, are also decreased by the presence of surfactants.

A nondimensional parameter β_L, which can be interpreted as a ratio of elastic forces to inertial forces, or as a ratio of a local convective time scale to a dissipative time scale, seems to characterize surfactant–turbulence interactions. Comparison of the current turbulence simulations with results from previous simulations of a vortex pair allow the conclusion that for $\beta_L \sim O(1)$, surfactants have a significant effect on surface turbulence, whereas an effectively clean surface can be obtained for $\beta_L < O(10^{-3})$.

Visualizations of the structure of turbulence at the free surface were performed for a weakly contaminated case and a highly contaminated surface. The weakly contaminated case showed a turbulence structure quite similar to the clean case which was investigated in earlier work. In this case, the surfactant concentration at the surface had large fluctuations which corresponded well with the surface divergence field. Regions of positive surface divergence, which can be associated with splatting events, were well correlated with large deficits of surfactant material. In the highly contaminated case, a steaky structure was found in the streamwise velocity field. It was speculated that this may be due to the large *fluctuating* surface shear stresses in this case which may give rise to local streamwise oriented surface structures. In this case the large surface elasticity suppressed fluctuations in surfactant concentration and in the surface divergence.

Acknowledgements

This work was supported by the Office of Naval Research through the Naval Research Laboratory. We also acknowledge the generous support of the DOD High Performance Computing Program.

References

[1] J. Lucassen, Longitudinal capillary waves Part 1. Theory, Trans. Faraday Soc. 64 (1968) 2221–2229.

[2] H.A. Espedal, O.M. Johannessen, J. Knulst, Satellite detection of natural films on the ocean surface, Geophys. Res. Lett. 23 (1996) 3151–3154.

[3] E.K. Rideal, On the influence of thin surface films on the evaporation of water, J. Phys. Chem. 29 (1925) 1585–1588.

[4] W.T. Tsai, Impact of a surfactant on a turbulent shear layer under the air–sea interface, J. Geophys. Res. 101 (1996) 28557–28568.

[5] J.R. Saylor, G.B. Smith, K.A. Flack, The effect of a surfactant monolayer on the temperature field of a water surface undergoing evaporation, Int. J. Heat Mass Transfer 43 (2000) 3073–3086.

[6] J.R. Saylor, G.B. Smith, K.A. Flack, Infrared imaging of the surface temperature field of water during film spreading, Phys. Fluids 12 (2000) 597–602.

[7] A.W. Adamson, Physical chemistry of surfaces, John Wiley, New York, 1990.

[8] P. Schluessel, W.J. Emery, H. Grassl, T. Mammem, On the bulk-skin temperature difference and its impact on satellite remote sensing of the sea surface temperature, J. Geophys. Res.—Oceans 95 (1990) 13341–13356.

[9] G.A. Wick, W.J. Emery, P. Schluessel, A comprehensive comparison between satellite measured skin and multichannel sea surface temperature, J. Geophys. Res.—Oceans 97 (1992) 5569–5595.

[10] W.J. Emery, Y. Yu, Satellite sea surface temperature patterns, Int. J. Remote Sens. 18 (1997) 323–334.

[11] R.A. Handler, G.B. Smith, R.I. Leighton, The thermal structure of an air–water interface at low wind speeds, Tellus A 53 (2001) 233–244.

[12] R.A. Handler, J.R. Saylor, R.I. Leighton, A.L. Rovelstad, Transport of a passive scalar at a shear-free boundary in fully developed turbulent open channel flow, Phys. Fluids 11 (1999) 2607–2625.

[13] R.A. Handler, T.F. Swean, R.I. Leighton, Length scales and the energy balance for turbulence near a free surface, AIAA J. 31 (1993) 1998–2007.

[14] T. Sarpakaya, Vorticity, free surfaces, and surfactants, Annu. Rev. Fluid Mech. 28 (1996) 83–128.

[15] W.R. Barger, A review of experimental observations and remaining questions concerning formation, persistence, and disappearance of sea slicks, Naval Research Laboratory Report 9313 (1991).

[16] R. Nagaosa, Direct numerical simulation of vortex structure and turbulent scalar transfer across a free surface in a fully developed turbulence, Phys. Fluids 11 (1999) 1581–1595.

[17] J.P. Boris, D.L. Book, Flux corrected transport I: SHASTA—A fluid transport code that works, J. Comp. Phys. 11 (1973) 38–69.

[18] S. Komori, H. Ueda, F. Ogino, T. Mizushina, Turbulence structure and transport mechanism at the free surface in an open channel flow, Int. J. Heat Mass Transfer 25 (1982) 513–521.

[19] S. Komori, R. Nagaosa, Y. Murakami, S. Chiba, K. Ishii, K. Kuwahara, Direct numerical simulation of three-dimensional open-channel flow with zero-shear gas–liquid interface, Phys. Fluids A 5 (1993) 115–125.

[20] Y. Pan, S. Banerjee, A numerical study of free surface turbulence in channel flow, Phys. Fluids 7 (1995) 1649–1664.

[21] R. Nagaosa, T. Saito, Turbulence structure and scalar transfer in stratified free-surface flows, AICHE J. 43 (1997) 2393–2404.

[22] M.J. Lee, J. Kim, P. Moin, Structure of turbulence at high shear rate, J. Fluid Mech. 216 (1990) 561–583.

[23] P.S. Bernard, J.M. Thomas, R.A. Handler, Vortex dynamics and the production of Reynolds stress, J. Fluid Mech. 253 (1993) 385–419.

[24] L.P. Bernal, J.T. Kwon, Vortex ring dynamics at a free surface, Phys. Fluids A 1 (1989) 449–451.

[25] G.B. Smith, R.J. Volino, R.A. Handler, R.I. Leighton, The thermal signature of a vortex pair impacting a free surface, J. Fluid Mech. 444 (2001) 49–78.

[26] C.T. Csanady, The role of breaking wavelets in air–sea gas transfer, J. Geophys Res. 95 (1990) 749–759.

[27] G.B. Smith, R.I. Leighton, A model for the aqueous thermal boundary layer at an air–water interface, Proceedings of IGARSS 2001, IEEE IGARSS, ISBN CD-ROM 0-7803-7033-3.